European Journal of Medicinal Chemistry 67 (2013) 175–187

Contents lists available at SciVerse ScienceDirect

European Journal of Medicinal Chemistry

journal homepage: http://www.elsevier.com/locate/ejmech

Original article

Lead identification of novel and selective TYK2 inhibitors

Jun Liang [b], Vickie Tsui [b], Anne Van Abbema [a,1], Liang Bao [b,2], Kathy Barrett [a], Maureen Beresini [a], Leo Berezhkovskiy [c], Wade S. Blair [a,3], Christine Chang [a], James Driscoll [c,4], Charles Eigenbrot [f], Nico Ghilardi [d], Paul Gibbons [b], Jason Halladay [c], Adam Johnson [a], Pawan Bir Kohli [a], Yingjie Lai [b], Marya Liimatta [a], Priscilla Mantik [e], Kapil Menghrajani [c], Jeremy Murray [f], Amy Sambrone [e], Yisong Xiao [g], Steven Shia [f], Young Shin [c], Jan Smith [a], Sue Sohn [d], Mark Stanley [b], Mark Ultsch [f], Birong Zhang [b], Lawren C. Wu [d], Steven Magnuson [b,*]

[a] Department of Biochemical and Cellular Pharmacology, Genentech, Inc., 1 DNA Way, South San Francisco, CA 94080, United States
[b] Department of Discovery Chemistry, Genentech, Inc., 1 DNA Way, South San Francisco, CA 94080, United States
[c] Department of Drug Metabolism and Pharmacokinetics, Genentech, Inc., 1 DNA Way, South San Francisco, CA 94080, United States
[d] Department of Immunology, Genentech, Inc., 1 DNA Way, South San Francisco, CA 94080, United States
[e] Department of Pharmaceutical Sciences, Genentech, Inc., 1 DNA Way, South San Francisco, CA 94080, United States
[f] Department of Structural Biology, Genentech, Inc., 1 DNA Way, South San Francisco, CA 94080, United States
[g] Department of Chemistry, WuXi Apptec, Waigaoqiao Free Trade Zone, Shanghai, PR China

ARTICLE INFO

Article history:
Received 8 December 2012
Received in revised form
28 March 2013
Accepted 31 March 2013
Available online 14 May 2013

Keywords:
Kinase inhibitor
Janus family kinase
Structure–activity relationship
Crystal structure
Hit to lead
Immunology

ABSTRACT

A therapeutic rationale is proposed for the treatment of inflammatory diseases, such as psoriasis and inflammatory bowel diseases (IBD), by selective targeting of TYK2. Hit triage, following a high-throughput screen for TYK2 inhibitors, revealed pyridine **1** as a promising starting point for lead identification. Initial expansion of 3 separate regions of the molecule led to eventual identification of cyclopropyl amide **46**, a potent lead analog with good kinase selectivity, physicochemical properties, and pharmacokinetic profile. Analysis of the binding modes of the series in TYK2 and JAK2 crystal structures revealed key interactions leading to good TYK2 potency and design options for future optimization of selectivity.

Abbreviations used: AcOH, acetic acid; ADME, absorption, distribution, metabolism, and excretion; aq., aqueous; TYK2BME, β-mercaptoethanol; Boc, *tert*-butyl carbamate; $CDCl_3$, deuterated chloroform; DCE, dichloroethane; DCM, dichloromethane; DMF, dimethylformamide; DMAP, 4-(*N*,*N*-dimethylamino)pyridine; DMSO, dimethylsulfoxide; DMSO-d_6, deuterated DMSO; DTT, dithiothreitol; EDCI, 1-ethyl-3-(3-dimethylaminopropyl) carbodiimide hydrochloride; ESI, electrospray ionization; h, hour; HATU, 2-(7-aza-1*H*-benzotriazole-1-yl)-1,1,3,3-tetramethyluronium hexafluorophosphate; HOBt, hydroxybenzotriazole; IV, intravenous; LCMS, liquid chromatography–mass spectrometry; $LogD_{7.4}$, log of partition coefficient between octanol and $pH_{7.4}$ aqueous buffer; MCT, methyl cellulose/tween; MDCK, Madin–Darby canine kidney cells; P_{app}, apparent permeability; Ph, phenyl; *p*-TsOH, *para*-toluenesulfonic acid; PO, by mouth; SCX-2, pre-packed Isolute® silica-based sorbent with a chemically bonded propylsulfonic acid functional group; SFC, supercritical fluid chromatography; TCEP, *tris*(2-carboxyethyl)phosphine; Tf, trifluorosulfonate; TFA, trifluoroacetic acid; THF, tetrahydrofuran; TLC, thin layer chromatography.

* Corresponding author. Tel.: +1 650 467 5325.
E-mail addresses: magnuson.steven@gene.com, stevenrm@gene.com (S. Magnuson).
[1] Current address: Department of Cell Biology, Novartis, Emeryville, CA, United States.
[2] Current address: ChemShuttle, Wuxi, PR China.
[3] Current address: Department of Infectious Disease, MedImmune, Gaithersburg, MD, United States.
[4] Current address: Department of Phamcokinetics, Theravance, South San Francisco, CA, United States.

0223-5234/$ – see front matter © 2013 Elsevier Masson SAS. All rights reserved.
http://dx.doi.org/10.1016/j.ejmech.2013.03.070

1. Introduction

1.1. TYK2 target biology

The Janus kinases (JAKs) are a family of four protein tyrosine kinases that associate with the intracellular domains of a wide range of cytokine and growth factor receptors that mediate inflammation and hematopoiesis [1]. Each of the four Janus kinases (JAK1, JAK2, JAK3, and TYK2) associates with a distinct set of receptors and induces intracellular signaling upon ligand binding by phosphorylating the receptor intracellular domains to generate docking sites for signal transducers and activators of transcription (STAT) proteins. STAT proteins are subsequently phosphorylated by the JAKs, form homodimers and heterodimers, and mediate gene transcription upon translocation to the cell nucleus.

The JAK family kinase TYK2 associates with several cytokine receptors, including those of the IL-12/IL-23 family, the IL-6 family, the IL-10 family, and the type I IFN family [1b,c,2]. Studies of TYK2-deficient mice [3] and a human patient lacking TYK2 protein [4] indicate that TYK2 protein is essential for the signaling of IL-12 and IL-23, which are associated with T helper type 1 (Th1) and T helper type 17 (Th17) inflammation, respectively [5]. IL-12 and IL-23 are heterodimeric proteins consisting of a common p40 subunit and a specific subunit of p35 for IL-12 and p19 for IL-23 (Fig. 1). The IL-12 and IL-23 receptors are heterodimeric receptors that share a common IL-12Rβ1 chain that pairs with either the IL-12Rβ2 chain for IL-12 [6] or the IL-23R for IL-23 [7]. The p40 subunit of IL-12 and IL-23 binds to IL-12Rβ1, whose intracellular domain associates with TYK2; whereas the p35 and p19 subunits of IL-12 and IL-23 bind to IL-12Rβ2 and IL-23R respectively, whose intracellular domains associate with JAK2. In response to stimulation with IL-12 or IL-23, the TYK2 and JAK2 enzymes phosphorylate the intracellular domains of the cytokine receptors, which in turn serve as docking sites for STAT proteins [8]. Subsequently, the TYK2 and JAK2 enzymes phosphorylate the STAT proteins, which then translocate into the nucleus where they regulate gene expression and transcription [1b,9]. Specifically, in the case of the IL-12 pathway, phosphorylation of STAT4 leads to expression of IFNγ [10] while in the IL-23 pathway, phosphorylation of STAT3 leads to increased IL-17 levels [7,11].

Th1 and Th17 immune responses and the IL-12/IL-23 pathways have been implicated in the pathogenesis of psoriasis and the inflammatory bowel diseases (IBD; Crohn's disease and ulcerative colitis), which are chronic inflammatory disorders of the skin (psoriasis) and gastrointestinal tract and colon (IBD) [12]. There is a strong genetic association of the IL-12 and IL-23 pathways with psoriasis and IBD [13] and substantial evidence for Th1 and Th17 inflammation in the skin and gut of patients with active disease [14]. Neutralization or genetic deficiency of IL-12 and IL-23 is efficacious in mouse models of psoriasis and IBD [15]. Moreover, antibodies against the p40 subunit of IL-12 and IL-23 are highly efficacious and approved for the treatment of psoriasis, and have shown efficacy in clinical studies in Crohn's disease [16]. Thus, inhibition of TYK2 kinase activity may be an effective therapeutic strategy for the treatment of psoriasis and IBD.

Therapies for psoriasis and IBDs must be safe. Therefore, inhibitors of TYK2 must have some degree of selectivity against JAK1, JAK2, and JAK3. JAK1 and JAK3 mediate the signaling of multiple receptors of the immune system. Deficiency of JAK1 results in perinatal lethality in mice with significant impairments in lymphopoiesis [17], whereas deficiency of JAK3 results in severe combined immunodeficiency in both mice and humans [18]. Although complete inhibition of the kinase activity of JAK1 and JAK3 is likely to be too broadly immunosuppressive, partial inhibition is tolerated in humans and is in fact efficacious for the treatment of rheumatoid arthritis and psoriasis [19]. Furthermore, it was recently reported that inhibition of JAK3 is not sufficient in blocking effects of immunologically relevant γc cytokines and that JAK1 is the dominant kinase [20]. JAK2 is important for the signaling of several hematopoietic growth factors, including the erythropoietin receptor that is responsible for the generation of red blood cells. Deficiency of JAK2 results in embryonic lethality in mice due to defective erythropoiesis [21], and therefore complete inhibition of the kinase activity of JAK2 will lead to anemia and other unacceptable effects on hematopoietic cells. On the basis of such safety considerations, we set forth to identify a TYK2 selective chemical series. In order to precisely measure TYK2 potency and JAK1- and JAK2-selectivity at both the enzyme and cell level, we had established biochemical and cell-based assays and determined that in cells, the predominant driver of IL-12, IL-6, and EPO pathway was TYK2, JAK1, and JAK2, respectively [22]. At the outset of the project, we were uncertain what the optimal level of JAK-family selectivity would be. We initially set a target of at least 10-fold in cell-based assays with the goal of obtaining compounds with a range of selectivity profiles that we could use to answer this important question.

1.2. Lead matter and chemical plan

A survey of the literature at the time we started the project revealed no TYK2 selective molecules, but there were a number of pan-JAK inhibitors [23] that would serve as control compounds as we identified new chemical matter. In order to identify potential chemistry starting points for a TYK2 small molecule inhibitor program, a high throughput screen (HTS) of the Genentech corporate collection was performed using an ATP-consumption assay [24]. Over 5000 primary hits [25] were identified and, after

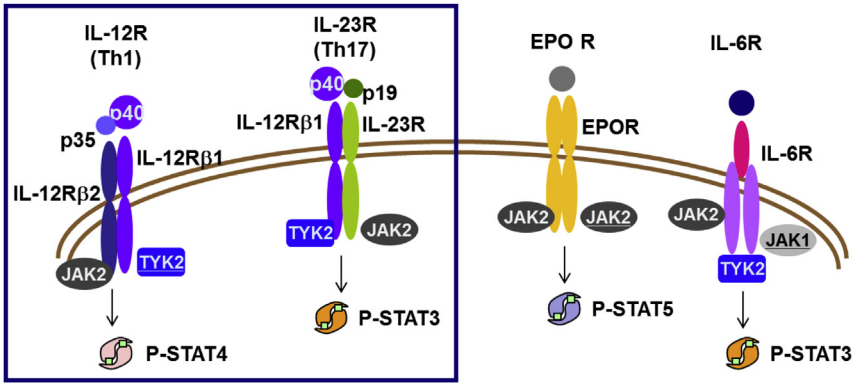

Fig. 1. Cytokines IL-12, IL-23, EPO, and IL-6 signaling pathways.

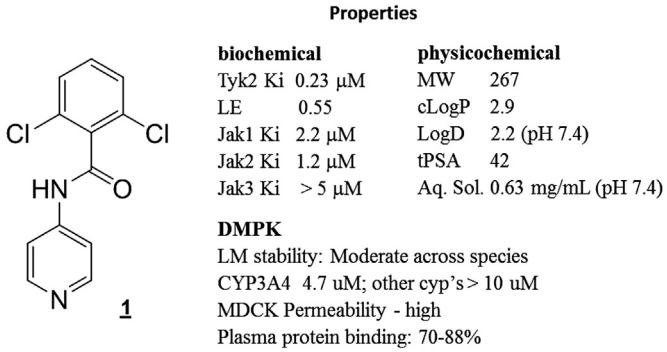

Fig. 2. Structure and properties of screening hit pyridine **1**.

clustering and a visual inspection of the hits, TYK2 IC50's, along with JAK1, 2 and 3 IC50's, were obtained on approximately 900 hits. To triage these 900 hits, chemical series and singletons were prioritized based on their potency, ligand efficiency, physicochemical properties, JAK kinase selectivity and general kinase selectivity. In choosing chemical series for initial hit expansion, priority was given to chemical series with good properties in all categories while compounds with poor data in multiple categories were set aside. In cases where a scaffold had a significant liability, but otherwise an attractive profile, the initial chemical plan, while establishing SAR, was designed to determine if the liability was addressable. Other properties, such as chemical tractability, possible binding modes, and novelty were considered, but more so factored into the initial chemical plan that was undertaken for hit expansion.

One hit that was of high interest to us was pyridine **1** (Fig. 2). This small, lead-like compound had very good potency (TYK2 K_i = 0.23 μM) for its size and thus excellent ligand efficiency (LE = 0.55) [26]. Physicochemical property space was generally good for a lead molecule [27], leaving ample opportunity to grow the molecule or install certain functional groups as we optimized potency. One concern with the physicochemical properties was the cLogP of 2.9. While this value in and of itself was not alarming, we recognized that we would not want the logP to climb much higher during optimization. The dichlorophenyl moiety of the molecule was the major contributor to the lipophilicity and we wanted to find less lipophilic alternatives early in the scaffold expansion. Pyridine **1** had been screened previously 13 times against other targets, including 9 other kinase targets and had only been identified as a hit once before. The compound was also a weak hit in a JAK2 HTS and during the TYK2 hit confirmation process, pyridine **1** was determined to have a 5-fold preference for TYK2 over closely-related JAK2, a 9-fold preference over JAK1, and greater than 20-fold selectivity over JAK3 [28,29]. This modest, but discernible selectivity over the other JAK kinases, was a key attribute that led to the selection of pyridine **1** for hit expansion. After resynthesis of the hit we tested it against a panel of 50 kinases at 1 μM [30] and found no other kinases with greater than 50% inhibition. Additionally, DMPK-related properties and thermodynamic solubility were very promising for this lead-like molecule.

At the time we began hit expansion of pyridine **1**, we did not have a crystal structure of compounds related to this scaffold bound to TYK2. We assumed that pyridine **1** was interacting with the TYK2 protein in the ATP binding pocket and determined that the hit was indeed competitive with ATP by doing the appropriate kinetic experiments [31]. For the docking of compound **1** (Fig. 3), we built a TYK2 homology model using a co-crystal structure of a literature pan-JAK inhibitor [28], whose structure on its own was very flat and had little three-dimensionality (see Supplemental data for details). The modeling predicted hydrogen bonding of the pyridine nitrogen to the backbone NH of Val981 in the hinge region. The dichlorophenyl group, which was connected to the core pyridine via an amide linker, was believed to extend back toward the P-loop. Even though the docked ligand was strained, we believed the general binding mode was correct, and small changes in the protein would relieve the ligand strain by allowing the 2,6-dichlorophenyl to be more orthogonal to the pyridine-amide moiety.

Our initial chemical plan was designed to understand the SAR of three different areas of the molecule. One area was the aforementioned lipophilic dichlorophenyl ring, where we intended to determine if alternate, less lipophilic substitutions were tolerated. We also planned to investigate whether the amide provided the best spatial and electronic linkage of the pyridine to the dichlorophenyl group. Lastly, we wanted to investigate the hinge binding pyridine and determine whether installation of an H-bond donor at the 2-position of the pyridine, thus creating an additional hinge interaction, would lead to a significant increase in potency. Based on modeling, there did not appear to be enough room to install an H-bond donor, other than perhaps $-NH_2$, toward the gatekeeper residue Met978 to interact with the backbone carbonyl of Glu979. Instead, it seemed more likely that a hydrogen bond donor would form an interaction with the backbone carbonyl of Val981, and extended functional groups linked with this H-bond donor would orient toward the solvent-exposed region.

2. Structure activity relationships

2.1. Dichlorophenyl region

While straightforward to investigate from a synthetic perspective, it proved difficult to identify less lipophilic substitutions than the 2,6-dichloro pattern on the phenyl ring while maintaining potency. A distinct preference for a 2,6-dihalo pattern (compounds **1**, **6**, **7**) found in the original hit was clear after analysis of the initial SAR (Table 1). Removal of both chlorine atoms (compound **2**) reduced activity by 10-fold while the analog with a single chlorine atom (compound **3**) was 5-fold less potent than the lead. Replacing the chlorine of compound **3** with a methyl (compound **4**), or

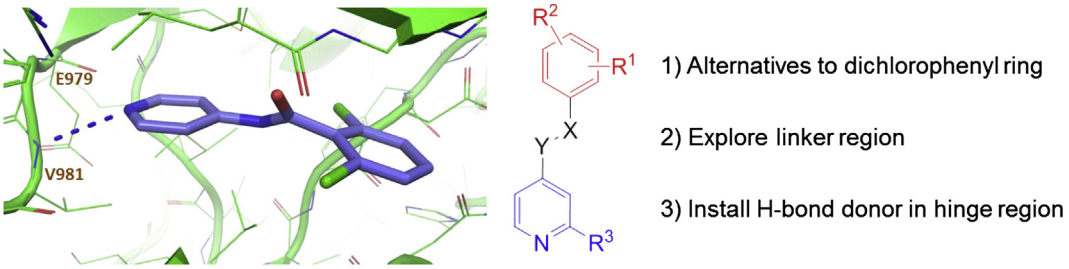

Fig. 3. Initial binding hypothesis of pyridine **1** and 3 regions for early scaffold expansion.

Table 1
Variation of dichlorophenyl ring.

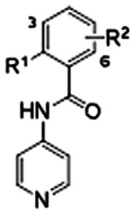

Ex	R^1	R^2	TYK2 K_i (μM)[a]	JAK1 K_i (μM)[a]	JAK2 K_i (μM)[a]
1	Cl	6-Cl	0.23	2.2	1.2
2	H	6-H	3.1	>3.5	3.2
3	Cl	6-H	1.1	>3.5	1.7
4	CH_3	6-H	2.4	>3.5	>3.5
5	CF_3	6-H	>3.5	>3.5	>3.5
6	Cl	6-F	0.23	1.7	2.0
7	F	6-F	0.54	3.1	2.8
8	Cl	6-CH_3	2.8	>3.5	>3.5
9	Cl	6-NH_2	>3.5	1.7	>3.5
10	Cl	6-CF_3	1.9	>3.5	>3.5
11	Cl	3-Cl	>3.5	>3.5	3.2
12	Cl	3-NH_2	>3.5	>3.5	>3.5
13	Cl	3-OCH_3	>3.5	>3.5	3.2
14	Cl	5-Cl	0.79	2.1	1.7
15	Cl	5-CF_3	0.90	2.0	1.8
16	Cl	5-OCH_3	2.8	>3.5	>3.5
17	Cl	4-Cl	1.2	4.6	3.0
18	Cl	4-CF_3	>3.5	>3.5	>3.5
19	Cl	4-NH_2	0.38	>3.5	3.2
20	Cl	4-OCH_3	3.2	>3.5	3.1

[a] Biochemical assays. Arithmetic mean of at least 3 separate determinations ($n \geq 3$). On average, the coefficients of variation were less than 0.3 times the mean for these assays.

trifluoromethyl (compound **5**) reduced activity. Setting chlorine as the preferred substitution at the 2-position, we investigated different substitutions around the phenyl ring. At the 6-position, introduction of a methyl, amino, or trifluoromethyl group (compounds **8**–**10**) was not as good as the 2,6-dichloro lead. Substitution at the 3-position was not beneficial (compounds **11**–**13**), but at the 5-position a chlorine substitution (compound **14**) and trifluoromethyl group (compound **15**) were well-tolerated with comparable or even slightly better potency than the unsubstituted comparator, compound **3**. Nevertheless, they were not more potent than the lead molecule, and did not accomplish the goal of reducing lipophilicity. Along these lines, the most promising vector on this ring was the 4-position, where an amino substitution (compound **19**) afforded good potency (TYK2 $K_i = 0.38$ μM) and was over a full log unit less lipophilic (cLogP = 1.6) than the 2,6-dichloro lead. Modeling, using the same homology model employed to predict the binding mode of compound **1** (Fig. 3), indicated that the phenyl group of compound **19** may be sitting under the tip of the P-loop with the 4-amino substitution pointed toward a polar region and specifically interacting with the backbone carbonyl of Glu905 (Fig. 4). While the aniline has potential liabilities, this result did encourage us to further explore this vector with other polar substituents during the lead optimization of this series. There was no notable improvement in JAK1 and JAK2 selectivity for the compounds in Table 1, but given the small modifications that were being made, this was perhaps not surprising.

2.2. Amide replacements

The second area of the molecule that we explored was the amide linker between the hinge-binding pyridine and the lipophilic

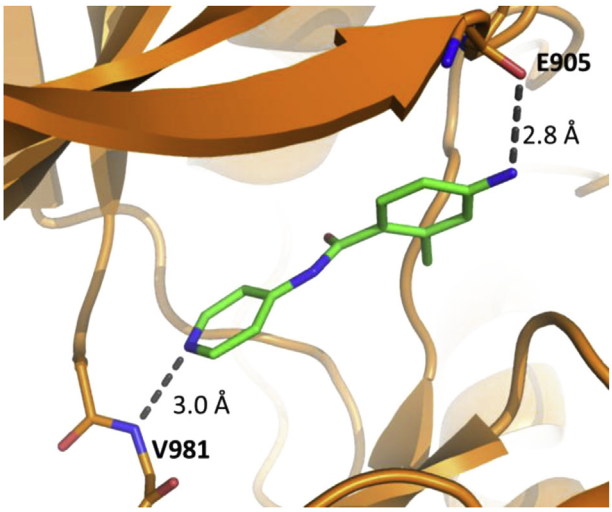

Fig. 4. Model of **19** interacting with the backbone carbonyl of Glu905 at the tip of P-loop.

dichlorophenyl ring (Table 2). The reverse amide (compound **21**) was only 5-fold less potent than the lead molecule indicating that there was some tolerance for altering the electronic nature of the linker. Conversely, the sulfonamide (compound **22**), reduced amide (compound **23**) and *N*-methyl amide (compound **24**) analogs were less active, indicating that the steric requirements were more significant in this region. Similarly, inserting a one atom extension into the linker (compound **25**) or installing heteroaromatic linkers (compounds **26**–**28**) were not acceptable substitutions for the amide. Based on this initial assessment, we continued to use the amide that was present in the HTS hit for further lead identification efforts.

2.3. Addition of hydrogen bond donor to hinge binding region

As anticipated, modifications to the pyridine ring, particularly installation of a hydrogen bond donor at the 2-position, had a more positive effect on TYK2 potency compared to changes to other regions of the molecule. Interestingly, two of the first analogs made, the unsubstituted 2-amino analog (compound **29**) and closely related *N*-methyl compound (analog **30**) were less potent than the parent analog lacking the hydrogen bond donor. In both cases, the decreased potency is likely due to increased basicity of the pyridine nitrogen when the hydrogen bond donor was added. The calculated pK_a [32] for the conjugate acid of the pyridine nitrogen in compound **1** is 5.8. Conversely, when the pyridine is substituted with a 2-NH_2 (compound **29**) or a 2-$NHCH_3$ (compound **30**), the calculated pK_a's for the conjugate acids of the pyridine nitrogen are 7.1 and 7.0, respectively. This indicates that a significant portion of these more basic pyridines may be protonated under the assay conditions (pH = 7.2), and this would result in weaker binding. When an NH-acetyl group was installed (compound **31**), the calculated pK_a for the conjugate acid of the pyridine nitrogen was 5.3, and in this case we observed a 15-fold improvement in TYK2 potency (Ki = 0.096 μM) compared to the *N*-methyl analog **30** (Ki = 1.5 μM). The conjugate acid of the pyridine nitrogen of sulfonamide **32** has a favorable calculated pK_a of 4.3, but this substitution was not tolerated in TYK2, presumably due to steric congestion of the bulkier sulfonamide in the hinge region. A number of very potent analogs (**34**, **36**–**38**) were obtained when different 6-membered heteroaromatics were added to the hydrogen bond donor. It is interesting to compare NH-4-pyrimdine **37** (TYK2 $K_i = 0.0048$ μM)

Table 2
Amide bond modifications.

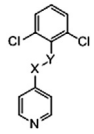

Ex	X–Y	TYK2 K_i (μM)[a]	JAK1 K_i (μM)[a]	JAK2 K_i (μM)[a]
1	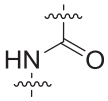	0.23	2.2	1.2
21	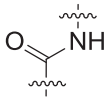	1.1	>3.5	>3.5
22	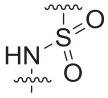	>3.5	>3.5	>3.5
23		>3.5	>3.5	>3.5
24	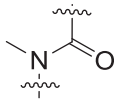	>3.5	>3.5	>3.5
25	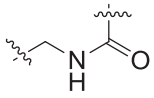	>3.5	>3.5	>3.5
26	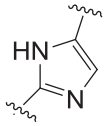	>3.5	>3.5	>3.5
27	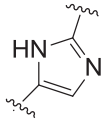	>3.5	>3.5	1.4
28	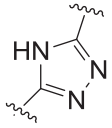	>3.5	>3.5	2.0

[a] Biochemical assays. Arithmetic mean of at least 3 separate determinations ($n \geq 3$). On average, the coefficients of variation were less than 0.3 times the mean for these assays.

to the NH-2-pyrimidine **35** (TYK2 K_i = 1.6 μM). The modeled binding mode of compound **37** (Fig. 5) places a favorable C–H in proximity to the backbone carbonyls of Val981 and P982 in the hinge region. Conversely, compound **35** is forced to place and unfavorable hydrogen bond accepting nitrogen in this region, thus explaining the 300-fold difference in potency of these compounds. It is also noteworthy to compare pyrimidine **37** to NH-phenyl analog **33** (TYK2 K_i = 0.14 μM). In this case, the 27-fold difference in potency can be attributed to N(3) of the pyrimidine in **37** eliminating a steric clash with the pyridine C(3)–H, that would be present with analog **33**. Avoiding this steric clash allows the rings of analog **37** to sit co-planar to one another and achieve a good fit in

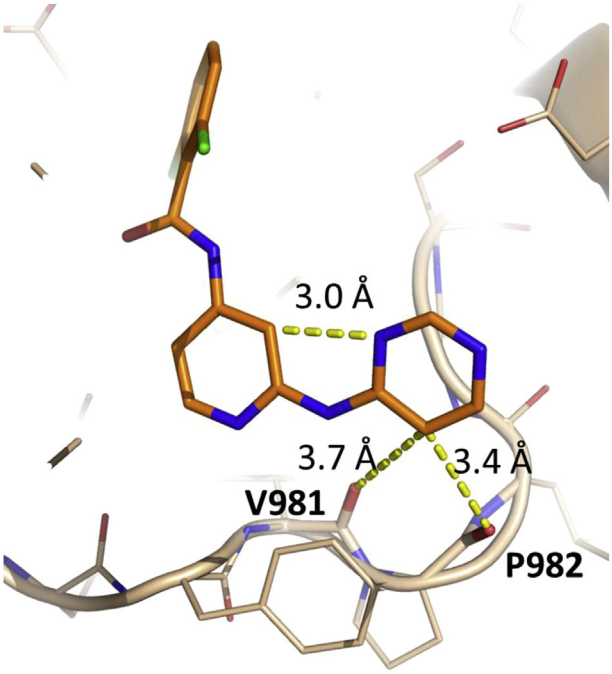

Fig. 5. Modeled binding mode for compound **37**.

the binding pocket (Fig. 5). Compound **37** was the most potent analog that we obtained in the initial expansion of the HTS hit but suffered from extremely high clearance in a rat PK study. An initial survey of 5-membered heterocycles, such as pyrazole **39**, was also undertaken but no significant benefit in terms of selectivity or clearance was obtained. Other functional groups were also investigated in our initial exploration of the hinge region. Inclusion of the hinge-binding pyridine in a bicyclic 7-azaindole bidentate hinge binder (compound **40**) was also well-tolerated, but use of this well-studied group [33] did not reveal any clear advantage to the other hinge binder options and was not investigated further. Pyridone **41** was equipotent (TYK2 K_i = 0.23 μM) to unsubstituted pyridine **1**, but this new analog was also 4-fold more potent against JAK2 (Ki = 0.060 μM). This compound was co-crystallized with the JH1 kinase domains of both TYK2 and JAK2 (Fig. 6) [34]. These crystal structures revealed that the interactions of the pyridone core were optimal with the hinge residues of JAK2, whereas such interactions were less optimal in the case of TYK2, due to a shift of the core away from the deep pocket. For example, the hydrogen bond donating pyridone nitrogen sat an ideal 2.8 Å away from the backbone carbonyl of GLU930 in JAK2, whereas the pyridone nitrogen sat 3.4 Å away from the backbone carbonyl of GLU979 in TYK2. With the shift away from the back pocket in TYK2, the hydrogen bond accepting pyridone oxygen is positioned closer to the backbone carbonyl of VAL981 than it is to backbone NH (3.1 vs. 3.4 Å), indicating the suboptimal positioning of the pyridone in TYK2. This shift may be due to different conformations between TYK2 and JAK2's gatekeeper methionine residues (MET978 and MET929, respectively). However, this residue is known to be flexible in both proteins as well as in other kinases with methionine gatekeepers, and specific causes of its differential conformation and flexibility is unknown.

2.4. NH-acetyl variation

In surveying all of these hinge binder modifications we felt that NH-acetyl **31** presented a unique opportunity in terms of ligand

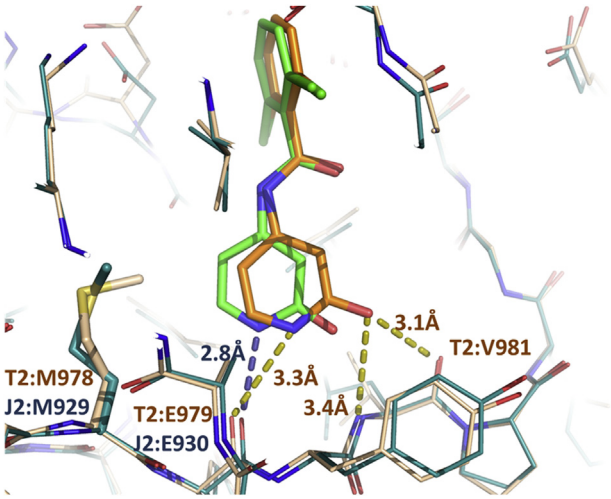

Fig. 6. Co-crystal structures of compound **41** with JAK2 (ligand in green, protein in blue) and with TYK2 (ligand in orange, protein in salmon). Selected distances between core atoms and hinge are shown, as well as names and numbers of relevant residues (TYK2 in deep orange, JAK2 in deep blue). (For interpretation of the references to color in this figure legend, the reader is referred to the web version of this article.)

efficiency (0.47) and physicochemical properties, and a more detailed investigation of NH-carbonyl substitutions was undertaken (Table 4). While an ethyl group (compound **42**) was well-tolerated, branched acyclic alkyls such as isopropyl and *t*-butyl (compounds **43** and **44**) were not favored. In contrast to the isopropyl substitution though, small cycloalkyls (compounds **46**–**48**) were favored, with cyclopropyl analog **46** being 19-fold more potent than methyl analog **31**. When heteroatoms were introduced into these small alkyl groups (compounds **50**–**53**), in an attempt to lower cLogP, a sharp drop-off in potency was observed. In addition to exploring different amides, we also investigated whether the amide functional group itself could be modified to related functional groups such as ureas and carbamates. These changes were indeed tolerated, as exemplified by the urea **54** and carbamate **55**, and provided another avenue for future lead optimization.

3. Synthesis

One obvious benefit of this lead scaffold was the straightforward synthesis of analogs. Exploration of the first area of interest – the dichlorophenyl ring – was easily accomplished through simple amide bond formation of 4-aminopyridine and a number of substituted benzoyl chlorides. Synthesis of HTS hit **1** is shown in Scheme 1, and specific conditions can be found in the Experimental section of the paper, while spectral data for compounds **2**–**20** can be found in the Supplemental information. In a similar fashion, analogs **21** and **25** (Table 2) were made by the appropriate coupling of an amine and an acid chloride (Supplemental data) while compound **22** was made by coupling 4-aminopyridine with 2,6-dichlorobenzene-1-sulfonyl chloride. Compound **23** was made by C=O reduction of the amide found in compound **1** using boron dimethyl sulfide complex, while compound **24** was made through *N*-methylation of compound **1** with sodium hydride and methyl iodide.

Compounds **26**–**28** (Table 2), where the linker amide was replaced by an isosteric heteroaromatic ring were made as shown in Scheme 2. Regioisomeric imidazoles **26** and **27** were easily formed in 1 step reactions by coupling of the appropriate amidine and bromomethyl ketone. Thus, compound **26** was made by coupling isonicotinimidamide with 2-bromo-1-(2,6-dichlorophenyl)ethanone, while analog **27** was synthesized through reaction of 2,6-dichlorobenenzenecarboximidamide and 2-bromo-1-(4-pyridinyl)ethanone. Compound **28** was made in a two-step route by first reacting 2,6-dichlorobenzoyl chloride with hydrazine, and then coupling the resulting hydrazide to 4-pyridine carbonitrile to afford the desired triazole **28**.

Table 3
Hinge binder modifications.

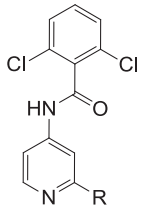

Ex	R	TYK2 K_i (μM)[a]	JAK1 K_i (μM)[a]	JAK2 K_i (μM)[a]
1	H	0.23	2.2	1.2
29	NH_2	0.93	>3.5	2.9
30	$NHCH_3$	1.5	>3.5	
31	NHC(O)CH3	0.096	2.9	0.31
32	$NHS(O)_2CH_3$	>3.5	>3.5	>3.5
33	NH-phenyl	0.14	>3.5	0.86
34	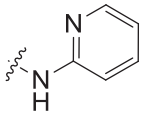	0.029	1.0	0.13
35	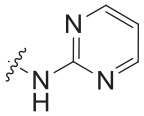	1.2	>3.5	2.5
36	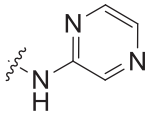	0.014	0.49	0.055
37	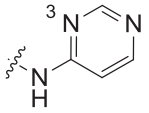	0.0049	0.20	0.020
38	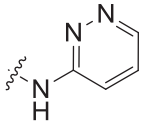	0.010	1.0	0.063
39	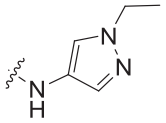	0.019	0.36	0.035
40[b]	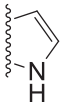	0.10	1.1	0.23
41[c]	OH	0.24	0.10	0.060

[a] Biochemical assays. Arithmetic mean of at least 3 separate determinations ($n \geq 3$). On average, the coefficients of variation were less than 0.3 times the mean for these assays.
[b] 5-Member ring fused to pyridine to form 7-azaindole hinge binder.
[c] Compound **41** adopts the pyridone tautomer.

Table 4
N-Acetyl variation.

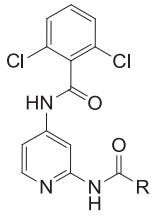

Ex	R	TYK2 K_i (μM)[a]	JAK1 K_i (μM)[a]	JAK2 K_i (μM)[a]
31	CH_3	0.096	2.9	0.31
42	CH_2CH_3	0.064	2.4	0.25
43	$CH(CH_3)_2$	0.84	>3.5	>3.5
44	$C(CH_3)_3$	>3.5	>3.5	>3.5
45	CH_2–cyclopropyl	0.094	>3.5	0.38
46	Cyclopropyl	0.0048	0.084	0.028
47	Cyclobutyl	0.074	1.5	0.51
48	Cyclopentyl	0.24	>3.5	2.4
49	Phenyl	2	>3.5	2.7
50	CH_2OH	0.25	>3.5	1.4
51	CH_2NH_2	1.2	>3.5	2.4
52	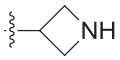	>3.5	>3.5	>3.5
53	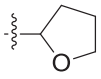	1.5	>3.5	1.3
54	$NHCH_2CH_3$	0.018	0.43	0.070
55	OCH3	0.17	2.6	0.61

[a] Biochemical assays. Arithmetic mean of at least 3 separate determinations ($n \geq 3$). On average, the coefficients of variation were less than 0.3 times the mean for these assays.

Synthesis of many of the analogs that probed addition of a second hinge binder (Tables 3 and 4) made use of bromopyridine intermediate **56** (Scheme 3) and aminopyridine **29**. Bromopyridine **56** itself was made by coupling 4-amino-2-bromopyridine to 2,6-dichlorobenzoyl chloride in the same way that compound **1** was made. Aminopyridine **29** could be made by either direct displacement of the bromide with ammonia under forcing conditions [35], or by reacting with lithium hexamethyldisilazide under Hartwig conditions [36], followed by acidic work-up. Buchwald coupling from bromide **56** was used to make NH-aryl and heteroaryl analogs **33**–**39**, as specifically exemplified for aminopyrimidine **37**. Amides **31**, and **42**–**53** were made from amine **29** by reacting with the appropriate acid chloride, as exemplified for cyclopropyl amide **46** or through other standard amide bond forming reaction [37]. Other analogs found in Tables 3 and 4 such as sulfonamide **32**, pyridone **41**, and urea **54**, were made using standard transformations similar to the ones discussed above and synthetic details can be found in the Supplemental material.

4. Lead compound properties

4.1. In vitro pharmacology

From all of the SAR generated in this initial survey of HTS hit pyridine **1**, cyclopropyl amide **46** clearly stood out and was profiled more extensively (Table 5). With a TYK2 K_i of 4.8 nM, its ligand efficiency (0.51) was comparable to the screening hit, and logD and solubility were still in acceptable range. In terms of biochemical selectivity, cyclopropyl amide **46** is 17-fold more potent at TYK2 than JAK1 and 6-fold more potent at TYK2 than JAK2 [28,38]. This level of selectivity is slightly better than the HTS hit **1**, and while the selectivity is admittedly subtle, the scaffold preferentially binds to TYK2 compared to other JAK kinases. Given the high homology of the JAK ATP binding sites, this was an important finding on which to build during lead optimization. To assess broader kinase selectivity, compound **46** was tested in a panel of 185 different kinases at a single point concentration of 500 nM (100× the TYK2 K_i) at Invitrogen. Only 7 other kinases (besides TYK2, JAK1 and JAK2) had >70% inhibition at this concentration, and after K_i determination, only CDK9 (111 nM) had a selectivity ratio of less than 50-fold (23-fold for CDK9 K_i/TYK2 K_i). The general kinase selectivity, while promising, would need to be continually monitored during lead optimization with particular attention to CDK9.

With compound **46** we had obtained sufficient biochemical potency to assess cell potency and see how cellular selectivity correlated with biochemical selectivity (Table 5). In NK92 cells, IL-12 stimulation leads to STAT4 phosphorylation in a TYK2-dependent fashion [22] and this was used to assess TYK2-dependent cell activity (see Supplemental data for experimental details). Compound **46** was approximately 100-fold less potent in the TYK2-dependent cell assay than it was in the TYK2 biochemical assay. The Km for ATP in the TYK2 biochemical assay is 10 μM so the 100-fold shift to the cell assay, where the intracellular ATP concentration is approximately 1 mM, was not unexpected [39]. To assess JAK1 and JAK2-dependent cell activity, IL-6 mediated STAT3 phosphorylation and Epo-mediated STAT5 phosphorylation assays,

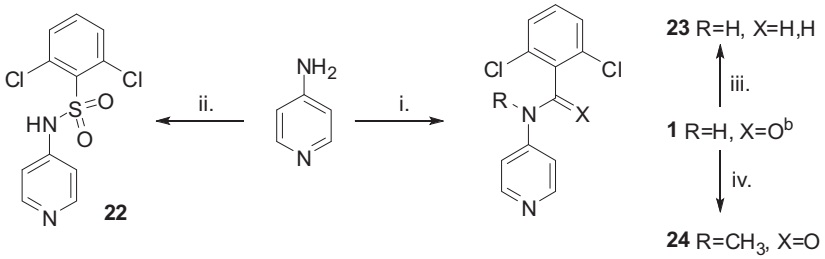

[a] Reagents and conditions: (i) 2,6-dichlorobenzoyl chloride, DMF, NEt_3, 95%; (ii) 2,6-dichlorobenzene-1-sulfonyl chloride, N-methylmorpholine, DMF, 15%; (iii) BH_3-SMe_2, THF, 44%; (iv) NaH, DMF; MeI, 67%. [b] Analogs **2**-**21** and **25** were made by analogous procedure to compound **1**, coupling appropriate amine and acid chloride.

Scheme 1. Synthesis of Analogs **1**–**25**.

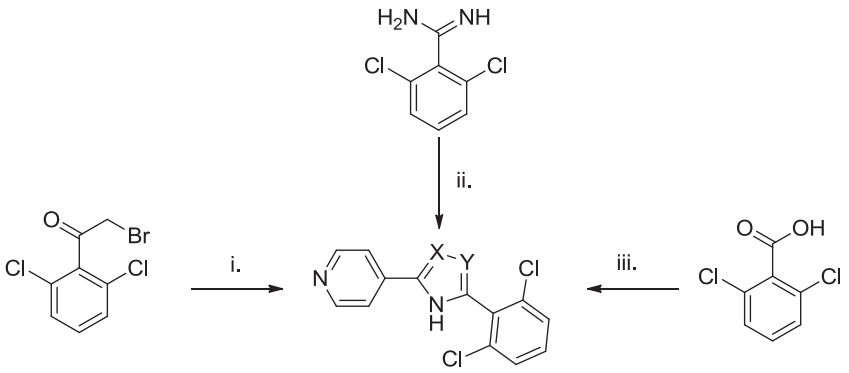

Rxn i: **26** (X=N, Y=H)
Rxn ii: **27** (X=H, Y=N)
Rxn iii: **28** (X=N, Y=N)

[a]Reagents and conditions: (i) isonicotinimidamide, sodium bicarbonate, dioxane, 100 °C, 17%; (ii) 2,6-dichlorobenenzenecarboximidamide, sodium bicarbonate, dioxane, 100 °C, 18%; (iii) hydrazine, NEt_3, dichloromethane, -78 °C to rt; 4-pyridine carbonitrile, sodium methoxide, 2-methoxyethanol, 130 °C, 29% for 2 steps.

Scheme 2. Synthesis of analogs **26**–**28**.

in TF-1 cells, were used respectively [22]. For cyclopropyl amide **46** there was reasonable agreement between biochemical selectivity and cell selectivity, with a small degradation in selectivity ratios in the cell assays. The JAK1 K_i/TYK2 K_i biochemical selectivity index of cyclopropyl amide **46** is 17-fold, but the ratio of IL6-mediated pSTAT3 (JAK1) EC_{50} over IL12-mediated pSTAT4 (TYK2) EC_{50} indicated only 5-fold cellular JAK1 selectivity. Similarly, the JAK2 K_i/TYK2 K_i biochemical selectivity index of compound **46** is 6-fold, but the ratio of Epo-mediated pSTAT5 (JAK2) EC_{50} over IL12-mediated pSTAT4 (TYK2) EC_{50} indicated only 4-fold cellular JAK2 selectivity. As mentioned in the introduction, we were not certain, at the outset of the project, what the optimal level of cellular selectivity was, but had set an initial target of 10-fold for TYK2 vs. both JAK1 and JAK2. While compound **46** had demonstrated meaningful cellular activity and selectivity, a major task during lead optimization would be to increase selectivity and deliver a set of

Table 5
Physicochemical and *in vitro* PD properties of compound **46**.

Physicochemical properties		*In vitro* potency and selectivity	
TYK 2 LE	0.51	TYK2 K_i	0.0048 μM
TYK2 LLE	4.9	JAK1 K_i (selectivity index)	0.084 μM (17-fold)
MW	350.2	JAK2 K_i (selectivity index)	0.028 μM (6-fold)
*t*PSA	71	IL12 – pSTAT4 EC_{50}[a,b]	0.38 μM
logD (pH 7.4)	3.4	IL6 – pSTAT3 EC_{50}[a,c] (cell selectivity index)	2.0 μM (5-fold)
Aqueous solubility (pH 7.4)	0.17 mg/mL	Epo – pSTAT5 EC_{50}[a,d] (cell selectivity index)	1.7 μM (4-fold)

[a] Cell-based assays. Arithmetic mean of at least 4 separate runs ($n \geq 4$). On average, the coefficients of variation were less than 0.5 times the mean for cell-based assays.
[b] Cell-based assay of TYK2 inhibition.
[c] Cell-based assay of JAK1 inhibition.
[d] Cell-based assay of JAK2 inhibition.

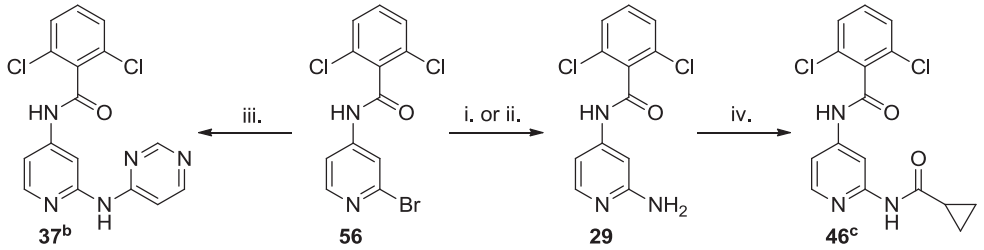

[a]Reagents and conditions: (i) aq. ammonia solution, autoclave 200 °C, 61%; (ii) $Pd_2(dba)_3$, DavePhos, lithium bis(trimethylsilyl)amide, 100 °C; NaOH, 65%; (iii) pyrimidine-4-amine, palladium acetate, Xantphos, cesium carbonate, microwave, 150 °C, 8%; (iv) cyclopropane carbonylchloride, pyridine, 50%. [b]Analogs **34-40** were made using similar conditions to those those used to make compound **38**. [c]Analogs **31** and **42-53** were made using similar conditions to those used to make compound **46**.

Scheme 3. Synthesis of analogs **31**, **33**–**39**, and **42**–**53**.

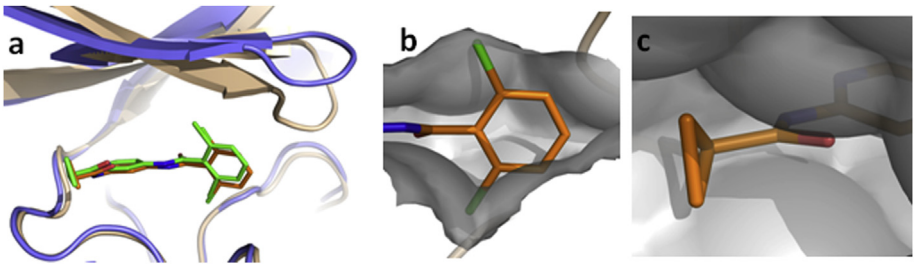

Fig. 7. a) Compound **46** co-crystallized with TYK2 (ligand in orange, protein in salmon) and JAK2 (ligand in green, protein in deep blue); b) Compound **46** with TYK2 – expanded view of dichlorophenyl region; c) Compound **46** with TYK2 – expanded view of cyclopropyl amide region. (For interpretation of the references to color in this figure legend, the reader is referred to the web version of this article.)

compounds with a range of selectivity to help determine, more definitively, the optimal level of TYK2 cellular selectivity over JAK1 and JAK2.

4.2. Structural biology

We were able to obtain both TYK2 and JAK2 crystal structures of compound **46** (Fig. 7a). A significant difference in these structures is the shape of the P-loop. In TYK2, the P-loop is more closed down whereas that of JAK2 is significantly more open. We believe this is not due to crystallographic artifacts because this has recently been observed by other investigators using different constructs as well [28,40]. This region is also not close to any asymmetric subunits. As a result of the exquisite shape of TYK2's P-loop, the dichlorophenyl ring is enclosed, fitting snugly in a pocket formed by the P-loop on the N-terminus and a small cavity in the C-terminus where the chlorine resides (Fig. 7b). The shape of the P-loop likely contributes to the TYK2 selectivity over JAK2 for compound **46**, and the small cavity in the C-terminus explains the tight SAR observed at the 2-position of the phenyl ring. On the other side of the molecule, the cyclopropyl group also fits snugly in a region that approaches the bulk solvent but does not pass the opening of the pocket (Fig. 7c). The dihedral angles from C2 and C3 on the cyclopropyl ring to the amide carbonyl oxygen are 40° and −30°, respectively. The center of the cyclopropyl ring has a dihedral angle with the carbonyl oxygen that is close to zero. This is the most frequently observed conformation of the cyclopropyl-amide in the Cambridge Structural Database [41] likely due to the special electronic characteristics of a cyclopropane [42]. Its unique conformation and small size explain the improved potency of **46** relative to analogs with isopropyl or larger cycloalkyl functional groups. Unlike the ethyl analog, the branched cyclopropyl group in this conformation is able to make van der Waals interactions with the N- and C-termini of the protein.

Table 6
In vitro and *in vivo* ADME properties of compound **46**.

In vitro ADME		*In vivo* rat and mouse PK[e]	
Micromsomal Cl_{hep} (mL/min/kg) (human, rat, mouse)[a]	8, 16, 64	Cl_{hep} (mL/min/kg) (rat, mouse)[f]	21, 65
Hepatocyte Cl_{hep} (mL/min/kg) (human, rat, mouse)[b]	7, 14, 51	$T_{1/2}$ (h) (rat, mouse)	1.2, 0.3
Cytochrome p_{450} inhibition (3A4, 2C9, 2C19, 1A4, 2D6)[c]	All > 10 μM	V_{ss} (L/h) (rat, mouse)	1.1, 1.2
MDCK permeability A:B P_{app} ($\times 10^{-6}$ cm/s)[d]	30	C_{max} (μM) (rat, mouse)[g]	2.5, 1.6
Plasma protein binding (%) (human, rat, mouse)	95, 96, 96	Bioavailability (%) (rat, mouse)	105, 73

[a] Predicted clearance from *in vitro* microsome preparations.
[b] Predicted clearance from cryopreserved rat hepatocytes.
[c] IC_{50} for inhibition of cytochrome P_{450}.
[d] Apparent permeability in MDCK transwell culture, A:B apical to basolateral.
[e] Animals dosed as 1 mg/kg IV and 5 mg/kg PO.
[f] Plasma clearance following *iv* dosing.
[g] Maximal plasma concentration following *po* dosing.

4.3. ADME properties

The ADME properties of analog **46** were also investigated and a summary of key data are included in Table 6. Predicted clearance from microsomes was moderate in human and rat with clearance at 38% and 29% of liver blood flow respectively. In mouse, clearance was higher (71% of liver blood flow), although clearance from mouse hepatocytes was slightly lower (56% of liver blood flow). *In vivo* clearance of Compound **46** was also assessed in rat and mouse PK through dosing at 1 mg/kg i.v. The measured clearance values *in vivo* (rat 21 mL/min/kg and mouse 65 mL/min/kg) were in good agreement with predicted *in vitro* clearance suggesting that extrahepatic mechanisms were not major routes of clearance for our compound. Compound **46** was also dosed at 5 mg/kg orally using a 5% methylcellulose formulation. The compound was absorbed well and this was reflected in the excellent bioavailability values of 105% and 73% for rat and mouse respectively. These *in vivo* PK parameters were also consistent with the high MDCK permeability and plasma protein binding that were observed *in vitro*. Taken in total, this was a very promising PK profile from which to launch a lead optimization effort, where reducing clearance was perhaps the most pressing concern.

5. Conclusions

While a number of patent applications describing identification of TYK2 inhibitors have published [43], this manuscript is the first detailed publication, to our knowledge, disclosing efforts to identify selective TYK2 inhibitors. Lead identification of HTS hit **1** proceeded efficiently to afford a number of potent TYK2 inhibitors with modest selectivity over JAK1 and JAK2. Cyclopropyl amide **46** demonstrated very good pharmacodynamic and pharmacokinetic properties and was a promising lead from which to launch a lead optimization effort. Efforts to improve potency and selectivity over JAK1 and JAK2, while maintaining good ADME properties will be the subject of a future publication.

6. Experimental protocols

6.1. General conditions

Unless otherwise indicated, all reagents and solvents were purchased from commercial sources and used without further purification. Moisture or oxygen sensitive reactions were conducted under an atmosphere nitrogen gas. Unless otherwise stated, ^{1}H spectra were recorded at room temperature using Varian Unity

Inova Bruker AVANCE III UltraShield-PlusTM Digital NMR spectrometer at indicated frequencies. Chemical shifts are expressed in ppm relative to an internal standard: tetramethylsilane (ppm = 0.00). The following abbreviations are used: br = broad signal, s = singlet, d = doublet, dd = doublet of doublets, t = triplet, q = quartet, m = multiplet. Purification by silica gel chromatography was carried out using a CombiFlash by Teledyne ISCO systems with pre-packed cartridges. Purification by reverse phase High Performance Liquid Chromatography (HPLC) was also used and the conditions were described as indicated. All final compounds were purified to >95% chemical purity, as assessed by HPLC (column: Agilent SD-C18, 2.1 × 30 mm, 1.8 μm; mobile phases: water with 0.5% TFA, CH_3CN with 0.5% TFA; flow rate: 0.4 mL/min; run time: 8.5 min; oven temperature: 40 °C: UV detection: 254 and 210 nm).

6.2. Representative procedures

6.2.1. 2,6-Dichloro-N-(pyridin-4-yl)benzamide (**1**)

To a round-bottom flask was added 4-aminopyridine (0.24 g, 2.55 mmol), followed by *N*,*N*-dimethylformamide (10 mL) and triethylamine (0.69 mL, 4.3 mmol). 2,6-dichlorobenzoyl chloride (0.5 g, 2.4 mmol) was added dropwise and the reaction mixture was stirred at 23 °C for 4 h. The mixture was poured into ice-water. The resulting precipitate was collected via filtration to give crude product which was purified by rpHPLC (Gilson 281; column: ASB C18, 150 × 25 mm, 5 μm; mobile phases: CH_3CN/aq. 0.01 M ammonium bicarbonate solution; flow rate: 25 mL/min) to afford the desired product (0.65 g, 95% yield). ^{1}H NMR (DMSO-d_6, 400 MHz) δ 11.21 (s, 1H), 8.47 (d, J = 6.0 Hz, 2H), 7.63 (d, J = 6.0 Hz, 2H), 7.57–7.47 (m, 3H). LCMS (ESI) m/z = 267.1 $[M + H]^+$.

6.2.2. 2,6-Dichloro-N-(pyridin-4-yl)benzenesulfonamide (**22**)

To a round-bottom flask was added 4-aminopyridine (0.15 g, 1.6 mmol), *N*,*N*-dimethylformamide (10 mL) and *N*-methylmorpholine (0.35 mL, 3.2 mmol) sequentially. 2,6-Dichlorophenylsulfonyl chloride (0.39 g, 1.6 mmol) was added dropwise and the reaction mixture was stirred at 23 °C for 4 h. The reaction mixture was poured into ice-water and was extracted with EtOAc (2 × 50 mL). Combined organics were dried over sodium sulfate and evaporated to dryness. The residue was purified by preparative TLC (10% MeOH/DCM) to afford the desired product (73.2 mg, 15% yield). ^{1}H NMR (DMSO-d_6, 400 MHz) δ 12.35 (s, 1H), 7.99 (d, J = 6.4 Hz, 2H), 7.49 (d, J = 7.6 Hz, 2H), 7.39 (t, J = 7.6 Hz, 1H), 6.85 (d, J = 7.2 Hz, 2H). LCMS (ESI) m/z = 302.8 $[M + H]^+$.

6.2.3. N-(2,6-Dichlorobenzyl)pyridin-4-amine (**23**)

2,6-Dichloro-*N*-(pyridin-4-yl)benzamide (0.5 g, 1.87 mmol) was dissolved in anhydrous. THF (20 mL) and borane dimethyl sulfide complex (0.4 mL, 6.8 mmol) was added. The reaction mixture was heated to reflux under nitrogen overnight. The next day, the reaction mixture was quenched by addition of methanol and extracted with EtOAc (2 × 20 mL). The combined organics were dried over sodium sulfate and evaporated to dryness. The residue was purified by silica gel column chromatography (0–10% MeOH/DCM) to afford the desired product (0.21 g, 44% yield). ^{1}H NMR (DMSO-d_6, 400 MHz) δ 8.07 (d, J = 6.4 Hz, 2H), 7.58 (bt, J = 4.4 Hz, 1H), 7.51 (d, J = 8.0 Hz, 2H), 7.39 (t, J = 8.0 Hz, 1H), 6.76 (d, J = 6.4 Hz, 2H), 4.49 (d, J = 4.4 Hz, 2H). LCMS (ESI) m/z = 252.9 $[M + H]^+$.

6.2.4. 2,6-Dichloro-N-methyl-N-(pyridin-4-yl)benzamide (**24**)

To a suspension of NaH (45 mg, 1.11 mmol) in anhydrous *N*,*N*-dimethylformamide (5 mL) was added 2,6-dichloro-*N*-(pyridin-4-yl)benzamide (0.1 g, 0.37 mmol) at 0 °C under nitrogen. After 30 min, methyl iodide (68 mg, 0.48 mmol) was added dropwise and the reaction mixture was stirred for an additional 4 h. The mixture was poured into the ice-water and the precipitate was collected to afford the desired product (70 mg, 67% yield). ^{1}H NMR (DMSO-d_6, 400 MHz) δ (2:1 mixture amide rotamers) 8.61 (dd, J = 1.6, 4.8 Hz, 1H), 8.42 (dd, J = 1.6, 4.8 Hz, 1H), 7.62–7.29 (m, 4H), 7.19 (dd, J = 4.8, 1.6 Hz, 1H), 3.40 (s, 2H), 3.17 (s, 1H). LCMS (ESI) m/z = 280.7 $[M + H]^+$.

6.2.5. 4-(5-(2,6-Dichlorophenyl)-1H-imidazol-2-yl)pyridine (**26**)

To a 10 mL round-bottom flask was added 2-bromo-1-(2,6-dichlorophenyl)ethanone (110 mg, 0.41 mmol) and 1,4-dioxane (1.0 mL). The white suspension was cooled to 0 °C under nitrogen and sodium carbonate (87 mg, 0.82 mmol) and isonicotinimidamide (50 mg, 0.40 mmol) were added sequentially. The reaction was heated to 100 °C and stirring was continued for two days when LCMS showed complete conversion. The mixture was cooled to room temperature, diluted with H_2O (10 mL) and extracted with EtOAc (2 × 10 mL). Combined organics were dried over Na_2SO_4, concentrated under reduced pressure and purified by rpHPLC (Gilson 215; column: Waters XBridge 30 × 100 mm, 10 μm; mobile phases: CH_3CN/water with 0.1% ammonia; flow rate: 60 mL/min) to give desired product (0.021 g, 18% yield). ^{1}H NMR (DMSO-d_6, 500 MHz) δ 13.21 (s, 1H), 8.66 (d, J = 5.1 Hz, 2H), 7.88 (d, J = 5.1 Hz, 2H), 7.65–7.40 (m, 4H). LCMS (ESI) m/z = 290.0 $[M + H]^+$.

6.2.6. 4-(2-(2,6-Dichlorophenyl)-1H-imidazol-5-yl)pyridine (**27**)

The title compound was made (17% yield) by coupling 2,6-dichlorobenenzenecarboximidamide and 2-bromo-1-(4-pyridinyl) ethanone using the same procedure that was used to make compound **26**. ^{1}H NMR (DMSO-d_6, 500 MHz) δ 12.78 (s, 1H), 8.51 (d, J = 5.0 Hz, 2H), 8.10 (s, 1H), 7.75 (d, J = 5.0 Hz, 2H), 7.64 (d, J = 9.0 Hz, 2H), 7.57 (dd, J = 9.0, 7.1 Hz, 1H). LCMS (ESI) m/z = 290.1 $[M + H]^+$.

6.2.7. 4-(5-(2,6-Dichlorophenyl)-4H-1,2,4-triazol-3-yl)pyridine (**28**)

Step 1. To a 100 mL round-bottom flask was added hydrazine (330 μL, 10 mmol), dichloromethane (20 mL) and triethylamine (1.2 mL, 8.9 mmol). The resulting solution was cooled to −78 °C and 2,6-dichlorobenzoyl chloride (1.7 g, 8.1 mmol) was added dropwise under nitrogen. The reaction mixture was stirred at −78 °C for one more hour and slowly warmed to room temperature over 2 h. The mixture was diluted with H_2O (50 mL) and extracted with dichloromethane (2 × 30 mL). The combined organic extracts were dried over sodium sulfate and concentrated under reduced pressure to give crude 2,6-dichlorobenzohydrazide which was directly carried to the next step.

Step 2. A 100 mL round-bottom flask was charged with crude 2,6-dichlorobenzohydrazide, followed by 2-methoxyethanol (10 mL), 4-pyridine carbonitrile (0.56 g, 5.4 mmol) and 25% sodium methoxide solution in methanol (0.56 mL, 2.7 mmol). The resulting brown suspension was heated at 130 °C under nitrogen for three days when LCMS showed complete conversion. The mixture was quenched with acetic acid (1 mL), diluted with 50 mL saturated sodium chloride solution, and extracted with EtOAc (2 × 50 mL). The combined organic extracts were dried over Na_2SO_4, concentrated under reduced pressure, and purified by rpHPLC to give desired product (0.46 g, 29% yield). ^{1}H NMR (DMSO-d_6, 500 MHz) δ 8.72 (d, J = 5.0 Hz, 2H), 7.98 (d, J = 5.0 Hz, 2H), 7.72–7.60 (m, 3H). LCMS (ESI) m/z = 291.0 $[M + H]^+$.

6.2.8. N-(2-Bromopyridin-4-yl)-2,6-dichlorobenzamide (**56**)

To a round-bottom flask was added sodium hydride (0.31 g, 7.82 mmol, 60% in mineral oil) and *N*,*N*-dimethylformamide (15 mL). The resulting suspension was cooled to 0 °C under nitrogen and then 2-bromopyridin-4-amine (0.74 g, 4.3 mmol) was added. The mixture was stirred at 0 °C for 20 min and then

2,6-dichlorobenzoyl chloride (0.82 g, 3.91 mmol) was added dropwise. The reaction was warmed to room temperature, stirred for 12 h, and then poured into ice-water (20 mL). The mixture was extracted with ethyl acetate (2 × 50 mL). The combined organic extracts were dried over Na_2SO_4 and concentrated under reduced pressure to afford crude desired product (1.0 g, 74% yield) that could be used without further purification. ^{1}H NMR (DMSO-d_6, 400 MHz): δ 11.41 (s, 1H), 8.33 (d, J = 5.6 Hz, 1H), 7.99 (d, J = 1.6 Hz, 1H), 7.64–7.54 (m, 4H). LCMS (ESI) m/z = 345.0 $[M + H]^+$.

*6.2.9. N-(2-Aminopyridin-4-yl)-2,6-dichlorobenzamide (**29**)*

Method 1: *N*-(2-bromopyridin-4-yl)-2,6-dichlorobenzamide (0.6 g, 1.7 mmol) was dissolved in an aq. ammonia solution (20 mL) and the mixture was heated to 200 °C in an autoclave for 16 h. After cooling to room temperature, the mixture was concentrated under reduced pressure. The residue was purified by silica gel column chromatography (0–10% MeOH/DCM) to afford the desired product (0.3 g, 61% yield). ^{1}H NMR (DMSO-d_6, 400 MHz) δ 10.71 (s, 1H), 7.79 (d, J = 5.6 Hz, 1H), 7.59–7.49 (m, 3H), 6.95 (s, 1H), 6.61 (d, J = 5.6 Hz, 1H), 5.91 (s, 1H). LCMS (ESI) m/z = 282.1 $[M + H]^+$.

Method 2: A 20 mL microwave tube was charged with *N*-(2-bromopyridin-4-yl)-2,6-dichlorobenzamide (346 mg, 1.00 mmol), $Pd_2(dba)_3$ (91.6 mg, 0.1 mmol) and 2-dicyclohexylphosphino-2′-(*N*,*N*-dimethylamino)biphenyl (DavePhos, 78.7 mg, 0.2 mmol). The tube was evacuated and back-filled with nitrogen three times before 1,4-dioxane (6 mL) and lithium bis(trimethylsilyl)amide (4.0 mL of 1.0 M solution in THF, 4.0 mmol) were added. The tube was sealed and heated at 100 °C for 5 h. The reaction mixture was cooled to room temperature, diluted with 1 N HCl (5 mL), and stirred for 10 min. The reaction mixture was adjusted to pH 12 using 1 N sodium hydroxide solution and then extracted with dichloromethane (3 × 30 mL). The combined organic extracts were dried over Na_2SO_4, and concentrated under reduced pressure. The residue was purified by silica gel column chromatography (0–10% MeOH/DCM) to afford the title compound (282 mg, 65% yield).

*6.2.10. 2,6-Dichloro-N-(2-(pyrimidin-4-ylamino)pyridin-4-yl) benzamide (**37**)*

A 20 mL microwave tube was charged with pyrimidin-4-amine (220 mg, 2.3 mmol), *N*-(2-bromopyridin-4-yl)-2,6-dichloro benzamide (1.2 g, 0.35 mmol), $Pd(OAc)_2$ (52 mg, 0.23 mmol), 4,5-bis(diphenylphosphino)-9,9-dimethylxantene (Xantphos, 0.27 g, 0.46 mmol), cesium carbonate (1.5 g, 4.6 mmol) and 1,4-dioxane (6 mL). The mixture was degassed with nitrogen. The tube was sealed, and heated by microwave at 150 °C for 20 min. The mixture was purified by silica gel column chromatography (0–15% DCM/MeOH) to afford the desired product (70 mg, 8.4% yield). ^{1}H NMR (DMSO-d_6, 400 MHz) δ 11.17 (s, 1H), 10.23 (s, 1H), 8.67 (s, 1H), 8.39 (d, J = 6.0 Hz, 1H), 8.21 (d, J = 5.6 Hz, 1H), 8.04 (s, 1H), 7.72 (d, J = 6.0 Hz, 1H), 7.59–7.51 (m, 3H), 7.37 (dd, J = 5.6, 1.6 Hz, 1H). LCMS (ESI) m/z = 360.0 $[M + H]^+$.

*6.2.11. 2,6-Dichloro-N-(2-(cyclopropanecarboxamido)pyridin-4-yl) benzamide (**46**)*

N-(2-Aminopyridin-4-yl)-2,6-dichlorobenzamide (0.5 g, 1.77 mmol) was dissolved in anhydrous pyridine (15 mL), and the mixture was cooled to 0 °C under nitrogen. Cyclopropanecarbonyl chloride (0.24 g, 2.3 mmol) was added dropwise and the reaction was warmed to room temperature. Stirring was continued for 4 h, and then the reaction was quenched with ice water (50 mL) and extracted dichloromethane (3 × 50 mL). The combined organic extracts were dried over Na_2SO_4 and concentrated under reduced pressure. The residue was purified by rpHPLC (Gilson GX 281; column: Phenomenx FA 150 × 30 mm; mobile phases: CH_3CN/H_2O with 0.1% TFA; flow rate: 25 mL/min; run time: 15 min) to afford the desired product (311 mg, 50% yield). ^{1}H NMR (DMSO-d_6, 400 MHz) δ 11.18 (s, 1H), 10.79 (s, 1H), 8.40 (d, J = 1.6 Hz, 1H), 8.23 (d, J = 5.6 Hz, 1H), 7.60–7.50 (m, 3H), 7.47 (dd, J = 5.6, 1.6 Hz, 1H), 2.02–1.98 (m, 1H), 0.81–0.79 (m, 4H). LCMS (ESI) m/z = 350.0 $[M + H]^+$.

Accession codes

PDB nos.: 4GFO for **41** complexed with TYK2D1023N, 4GFM for **41** complexed with JAK2, 4GIH for **46** complexed with TYK2-combo, 4GMY for **46** complexed with JAK2.

Acknowledgment

We thank, Mengling Wong, Chris Hamman, Michael Hayes, Baiwei Lin, Deven Wang, Yutao Jiang, and Yanzhou Liu for purification and analytical support; Daniel Hascall, Grady Howes, Gigi Yuen, and Garima Porwal for compound management support; Hoa Le and Qin Yue for ADME support; Emile Plise and Jonathan Cheng for MDCK data; Ning Liu for microsomal stability; Jasleen Sodhi for reversible CYP inhibition measurement; Quynh Ho for plasma protein binding measurement.

Diffraction data were collected at the Stanford Synchrotron Radiation Lightsource, operated for the U.S. Department of Energy Office of Science by Stanford University. The SSRL Structural Molecular Biology Program is supported by the DOE Office of Biological and Environmental Research, National Institute of General Medical Sciences (NIH) (including P41GM103393) and the National Center for Research Resources (P41RR001209).

Appendix A. Supplementary data

Supplementary data related to this article can be found at http://dx.doi.org/10.1016/j.ejmech.2013.03.070.

References

[1] (a) K. Ghoreschi, A. Laurence, J.J. O'Shea, Janus kinases in immune cell signaling, Immunological Reviews 228 (2009) 273;
(b) W.J. Leonard, J.J. O'Shea, Jaks and STATs: biological implications, Annual Review of Immunology 16 (1998) 293;
(c) K.D. Liu, S.L. Gaffen, M.A. Goldsmith, Jak/STAT signaling by cytokines, Current Opinion in Immunology 10 (1998) 271.

[2] J.N. Ihle, B.A. Witthuhn, F.W. Quelle, K. Yamamoto, O. Silvennoinen, Signaling through the hematopoietic cytokine receptors, Annual Review of Immunology 13 (1995) 369.

[3] (a) M. Karaghiosoff, H. Neubauer, C. Lassnig, P. Kovarik, H. Schindler, H. Pircher, B. McCoy, C. Bogdan, T. Decker, G. Brem, K. Pfeffer, M. Muller, Partial impairment of cytokine responses in Tyk2-deficeint mice, Immunity 13 (2000) 549;
(b) K. Shimoda, K. Kato, K. Aoki, T. Matsuda, A. Miyamoto, M. Shibamori, M. Yamashita, A. Numata, K. Takase, S. Kobayashi, S. Shibata, Y. Asano, K. Sekiguchi, K. Nakayama, T. Nakayama, T. Okamura, S. Okamara, Y. Niho, K. Nakayama, Tyk2 plays a restricted role in IFNα signaling, although it is required for IL-12-mediated T cell function, Immunity 13 (2000) 561;
(c) M.H. Shaw, V. Boyartchuck, S. Wong, M. Karaghiosoff, J. Ragimbeau, S. Pellegrini, M. Muller, W.F. Dietrich, G.S. Yap, A natural mutation in the Tyk2 pseudokinase domain underlies altered susceptibility of B10.Q/J mice to infection and autoimmunity, Proceedings of the National Academy of Sciences of the United States of America 100 (2003) 11594.

[4] Y. Minegishi, M. Saito, T. Morio, K. Watanabe, K. Agematsu, S. Tsuchiya, H. Takada, T. Hara, N. Kawamura, T. Ariga, H. Kaneko, N. Kondo, I. Tsuge, A. Yachie, Y. Sakiyama, T. Iwata, F. Bessho, T. Ohishi, K. Joh, K. Imai, K. Kogawa, M. Shinohara, M. Fujieda, H. Wakiguchi, S. Pasic, M. Abinun, H.D. Ochs, E.D. Renner, A. Jansson, B.H. Belohradsky, A. Melin, N. Shimizu, S. Mizutani, T. Miyawaki, S. Nonoyama, H. Karasuyama, Human tyrosine kinase 2 deficiency reveals its requisite roles in multiple cytokine signals involved in innate and acquired immunity, Immunity 25 (2006) 745.

[5] (a) D. Mucida, H. Cheroutre, The many face-lifts of CD4 T helper cells, Advances Immunology 107 (2010) 139;
(b) M.K. Gately, L.M. Renzetti, J. Magram, A.S. Stern, L. Adorini, U. Guber, D.H. Presky, The interleukin-12/interleukin-12-receptor system: role in

normal and pathologic immune responses, Annual Review of Immunology 16 (1998) 495;
(c) W.T. Watford, B.D. Hissong, J.H. Bream, Y. Kanno, L. Muul, J.J. O'Shea, Signaling by IL-12 and IL-23 and the immunoregulatory roles of STAT4, Immunological Reviews 202 (2004) 139;
(d) K. Boniface, B. Blom, Y.-J. Liu, R.D.W. Maleft, From interleukin-23 to T-helper 17 cells: human T-helper cell differentiation revisited, Immunological Reviews 226 (2008) 132;
(e) C.A. Hunter, New IL-2 family members: IL-23 and IL-27, cytokines with divergent functions, Nature Reviews Immunology 5 (2005) 521;
(f) C.L. Langrish, B.S. McKenzie, N.J. Wilson, R.D.W. Malefyt, R.A. Kastelein, D.J. Cua, IL-12 and IL-23: master regulators of innate and adaptive immunity, Immunological Reviews 202 (2004) 96;
(g) G. Trinchieri, S. Pflanz, R.A. Kastelein, The IL-12 family of heterodimeric cytokines: new players in the regulation of T cell responses, Immunity 19 (2003) 641.

[6] (a) A.O. Chua, R. Chizzonite, B.B. Desai, T.P. Truitt, P. Nunes, L.J. Minetti, R.R. Warrier, D.H. Presky, J.F. Levine, M.K. Gately, U. Gubler, Expression cloning of a human IL-12 receptor component, Journal of Immunology 153 (1994) 128;
(b) D.H. Presky, H. Yang, L.J. Minetti, A.O. Chua, N. Nabavi, C.-Y. Wu, M.K. Gately, U. Gubler, A functional interleukin 12 receptor complex is composed of two β-type cytokine receptor subunits, Proceedings of the National Academy of Sciences of the United States of America 93 (1996) 14002.

[7] C. Parham, M. Chirica, J. Timans, E. Vaisberg, M. Travis, J. Cheung, S. Pflanz, R. Zhang, K. Singh, F. Vega, W. To, J. Wagner, A.-M. O'Farrell, T. McClanahan, S. Zurawski, C. Hannum, D. Gorman, D. Rennick, R.A. Kastlein, R.D.W. Maleft, K.W. Moore, A receptor for the heterodimeric cytokine IL-23 is composed of IL-12β1 and a novel cytokine receptor subunit, IL-23R, Journal of Immunology 168 (2002) 5699.

[8] (a) C.M. Bacon, E.F. Petricoin III, J.R. Ortaldo, R.C. Rees, A.C. Larner, J.A. Johnson, J.J. O'Shea, Interleukin 12 induces tyrosine phosphorylation and activation of STAT4 in human lymphocytes, Proceedings of the National Academy of Sciences of the United States of America 92 (1995) 7307;
(b) B. Oppmann, R. Lesley, B. Blom, J.C. Timans, Y. Xu, B. Hunte, F. Vega, N. Yu, J. Wang, K. Singh, F. Zonin, E. Vaisberg, T. Churakova, M. Liu, D. Gorman, J. Wagner, S. Zurawski, Y.-J. Liu, J.S. Abrams, K.W. Moore, D. Rennick, R.D.W. Maleft, C. Hannum, J.F. Bazan, R.A. Kastelein, Novel p19 protein engages IL-12p40 to form a cytokine, IL-23, with biological activities similar as well as distinct from IL-12, Immunity 13 (2000) 715.

[9] M.M. Brierley, E.N. Fish, STATs: multifaceted regulators of transcription, Journal of Interferon & Cytokine Research 23 (2005) 733.

[10] (a) W.E. Thierfelder, J.M. van Deursen, K. Yamamoto, R.A. Tripp, S.R. Sarawar, R.T. Carson, M.Y. Sangster, D.A.A. Vignali, P.C. Doherty, G.C. Grosveld, J.N. Ihle, Requirement for STAT4 in interleukin-12-mediated response of natural killer and T cells, Nature 382 (1996) 171;
(b) M.H. Kaplan, Y.-L. Sun, T. Hoey, M.J. Grusby, Impaired IL-12 responses and enhanced development of Th2 cells in STAT4-deficient mice, Nature 382 (1996) 174.

[11] S. Aggarwal, N. Ghilardi, M.-H. Xie, F.J. de Sauvage, A.L. Gurney, Interleukin-23 promotes a distinct CD4 T cell activation state characterized by the production of interleukin-17, Journal of Biological Chemistry 278 (2003) 1910.

[12] (a) P. Miossec, T. Korn, V.K. Kuchroo, Interleukin-17 and type 17 helper cells, The New England Journal of Medicine 361 (2009) 888;
(b) J. Louten, K. Boniface, R.D.W. Malefyt, Development and function of Th17 cells in health and disease, Journal of Allergy Clinical Immunology 123 (2009) 1004;
(c) W. Ouyang, J.K. Kolls, Y. Zheng, The biological functions of T helper 17 cell effector cytokines in inflammation, Immunity 28 (2008) 454;
(d) P.P. Ahem, A. Izcue, K.J. Maloy, F. Powrie, The interleukine-23 axis in intestinal inflammation, Immunological Reviews 226 (2008) 147.

[13] (a) J.H. Cho, The genetics and immunopathogenesis of inflammatory bowel disease, Nature Reviews Immunology 8 (2008) 458;
(b) R.P. Nair, K.C. Duffin, C. Helms, J. Ding, P.E. Stuart, D. Goldgar, J.E. Gudjonsson, Y. Li, T. Tejasvi, B.-J. Feng, A. Ruether, S. Schreiber, M. Weichenthal, D. Gladman, P. Rahman, S.J. Schrodi, S. Prahalad, S.L. Guthery, J. Fischer, W. Liao, P.-Y. Kwok, A. Menter, G.M. Lathrop, A. Carol, G.A. Wise, A.B. Begovich, J.J. Voorhees, J.T. Elder, G.G. Krueger, A.M. Bowcock, G.R. Abecasis, Genome-wide scan reveals association of psoriasis with IL-23 and NF-κB pathways, Nature Genetics 41 (2009) 199;
(c) M. Cargill, S.J. Schrodi, M. Chang, V.E. Garcia, R. Brandon, K.P. Callis, N. Matsunami, K.G. Ardlie, D. Civello, J.J. Catanese, D.U. Leong, J.M. Panko, L.B. McAllister, C.B. Hansen, J. Papenfuss, S.M. Prescott, T.J. White, M.F. Leppert, G.G. Krueger, A.B. Begovich, A large-scale genetic association study confirmed IL12b and leads to the identification of IL23R as psoriasis-risk gene, American Journal of Human Genetics 80 (2007) 273;
(d) F. Capon, P. Di Meglio, N.J. Szaub, N.J. Prescott, C. Dunster, L. Baumber, K. Timms, A. Gutin, V. Abkevic, A.D. Burden, J. Lanchbury, J.N. Barker, R.C. Trembath, F.D. Nestle, Sequence variants in the genes for the interleukin-23 receptor (IL23R) and its ligand (IL12b) confer protection against psoriasis, Human Genetics 122 (2007) 201;
(e) R.J. Duerr, K.D. Taylor, S.R. Brant, J.D. Rioux, M.S. Silverberg, M.J. Daly, A.H. Steinhart, C. Abraham, M. Regueiro, A. Griffiths, T. Dassopoulos, A. Bitton, H. Yang, S. Targan, L.W. Datta, E.O. Kistner, L.P. Schumm, A.T. Lee, P.K. Gregersen, M.M. Barmada, J.I. Rotter, D.L. Nicolae, J.H. Cho, A genome-wide association study identifies IL23R as an inflammatory bowel disease gene, Science 314 (2006) 1461.

[14] (a) N. Yawalkar, S. Karlen, R. Hunger, C.U. Brand, L.R. Braathen, Expression of interleukin-12 is increased in psoriatic skin, Journal of Investigative Dermatology 111 (1998) 1053;
(b) E. Lee, W.L. Trepiccio, J.L. Oestreicher, D. Pittman, F. Wang, F. Chamian, M. Dhodapkar, J.G. Krueger, Increased expression of interleukin 23 p19 and p40 in lesional skin of patients with psoriasis vulgaris, Journal of Experimental Medicine 199 (2004) 125;
(c) G. Piskin, R.M.R. Sylva-Steenland, J.B. Bos, M.B.M. Teunissen, *In vitro* and *in situ* expression of IL-23 by keratinocytes in healthy skin and psoriasis lesions: enhanced expression in psoriatic skin, Journal of Immunology 176 (2006) 1908;
(d) G. Monteleone, L. Biancone, R. Marasco, G. Morrone, O. Marasco, F. Luzza, F. Pallone, Interleukin 12 is expressed and actively released by Crohn's disease intestinal lamina propria mononuclear cells, Gastroenterology 112 (1997) 1169;
(e) D. Berrebi, M. Besnard, G. Fromont-Hankard, R. Paris, J.F. Mougenot, P. De Lagausie, D. Emilie, J.P. Cezard, J. Navarro, M. Peuchmaur, Interleukin-12 expression is focally enhanced in the gastric muscosa of pediatric patients with Crohn's disease, American Journal of Pathology 152 (1998) 667;
(f) V. Holtta, P. Klemetti, T. Sipponen, M. Westerholm-Ormio, G. Kociubinski, H. Salo, L. Rasanen, K.-L. Kolho, M. Farkkila, E. Savilahti, O. Vaaraia, IL-23/IL-17 immunity as a hallmark of Crohn's disease, Inflammatory Bowel Disease 14 (2008) 1175;
(g) J. Pene, S. Chevalier, L. Preisser, E. Venereau, M.-H. Guilleux, S. Ghannam, J.-P. Moles, Y. Danger, E. Ravon, S. Lesaux, H. Yssel, H. Gascan, Chronically inflamed human tissues are infiltrated by highly differentiated Th17 lymphocytes, Journal of Immunology 180 (2008) 7423.

[15] (a) L. van der Fits, S. Mourits, J.S.A. Voerman, M. Kant, L. Boon, J.D. Laman, F. Cornelissen, A.-M. Mus, E. Florencia, E. Prens, E. Lubberts, Imiquimod-induced psoriasis-like skin inflammation in mice is mediated via the IL-23/IL-17 axis, Journal of Immunology 182 (2009) 5836;
(b) H.-L. Ma, S. Liang, J. Li, L. Napierata, T. Brown, S. Benoit, M. Senices, D. Gill, K. Dunussi-Joannopoulos, M. Collins, C. Nickerson-Nutter, L.A. Fouser, D.A. Yong, IL-22 is required for Th17 cell-mediated pathology in a mouse model of psoriasis-like skin inflammation, Journal of Clinical Investigation 118 (2008) 597;
(c) C.O. Elson, Y. Cong, C. Weaver, T.R. Schoeb, T.K. McClanahan, R.B. Fick, R.A. Kastelein, Monoclonal anti-interleukin 23 reverses active colitis in a T cell-mediated model in mice, Gastroenterology 132 (2007) 2359;
(d) S. Hue, P. Ahern, S. Buonocore, M.C. Kullberg, D.J. Cua, B.S. McKenzie, F. Powrie, K.J. Maloy, Interleukin-23 drives innate and T cell-mediated intestinal inflammation, Journal of Experimental Medicine 203 (2006) 2473;
(e) M.C. Kullberg, D. Jankovic, C.G. Feng, S. Hue, P. Gorelick, B.S. McKenzie, D.J. Cua, F. Powrie, A.W. Cheever, K.J. Maloy, A. Sher, IL-23 plays a key role in Helicobbacter-induced T cell-dependent colitis, Journal of Experimental Medicine 203 (2006) 2485;
(f) H.H. Uhlig, B.S. McKenzie, S. Hue, C. Thompson, B. Joyce-Shaikh, R. Stephankova, N. Robinson, S. Buonocore, H. Tlaskalova-Hogenova, D.J. Cua, F. Powrie, Differential activity of IL-12 and IL-23 in mucosal and systemic innate immune pathology, Immunity 25 (2006) 309;
(g) D. Yen, J. Cheung, H. Scheerens, F. Poulet, T. McClanahan, B.S. McKenzie, M.A. Kleinschek, A. Owyang, J. Mattson, W. Blumenschein, E. Murphy, M. Sathe, D.J. Cua, R.A. Kastelein, D. Rennick, IL-23 is essential for T cell-mediated colitis and promotes inflammation via IL-17 and IL-6, Journal of Clinical Investigation 116 (2006) 1310;
(h) N.J. Davidson, S.A. Hudak, R.E. Lesley, S. Mennon, M.W. Leach, D.M. Rennick, IL-12, but not IFNγ, plays a major role in sustaining the chronic phase of colitis in IL-10-deficient mice, Journal of Immunology 161 (1998) 3143.

[16] (a) J.M. Benson, C.W. Sachs, G. Treacy, H. Zhou, C.E. Pendley, C.M. Brodmerkel, G. Shankar, M.A. Mascelli, Therapeutic targeting of IL-12/23 pathways: generation and characterization of ustekinumab, Nature Biotechnology 29 (2011) 615;
(b) L. Steinman, Mixed results with modulation of Th-17 cells in human autoimmune diseases, Nature Immunology 11 (2010) 41.

[17] S.J. Rodig, M.A. Meraz, J.M. White, P.A. Lampe, J.K. Riley, C.A. Arthur, K.L. King, K.C.F. Sheehan, L. Yin, D. Pennica, E.M. Johnson, R.D. Schreiber, Disruption of the Jak1 gene demonstrates obligatory and nonredundant roles of the Jaks in cytokine-induced biologic response, Cell 93 (1998) 373.

[18] (a) F. Candotti, S.A. Oakes, J.A. Johnson, S. Giliani, R.F. Schumacher, P. Mella, M. Fioini, A.G. Ugazio, R. Badolato, L.D. Notarangelo, F. Bozzi, P. Macchi, D. Strina, P. Vezzoni, R.M. Blaese, J.J. O'Shea, A. Villa, Structural and functional basis for Jak3-deficient severe combined immunodeficiency, Blood 90 (1997) 3996;
(b) S.M. Russell, N. Tayebi, H. Nakajima, M.C. Riedy, J. Roberts, M.J. Aman, T.-S. Migone, M. Noguchi, M.L. Markert, R.H. Buckley, J.J. O'Shea, W.J. Leonard, Mutation of Jak3 in a patient with SCID: essential role of Jak3 in lymphoid development, Science 270 (1995) 797;
(c) P. Macchi, A. Villa, S. Giliani, M.G. Sacco, A. Frattini, F. Porta, A.G. Ugazio, J.A. Johnson, F. Candotti, J.J. O'Shea, P. Vezzoni, L.D. Notarangelo, Mutations of Jak-3 gene in patients with autosomal severe combined immune deficiency, Nature 377 (1995) 65;

(d) D.C. Thomis, C.B. Gurniak, E. Tivol, A.H. Sharpe, L.J. Berg, Defects in B lymphocyte maturation and T lymphocyte activation in mice lacking Jak3, Science 270 (1995) 794;
(e) T. Nosaka, J.A. van Deursen, R.A. Tripp, W.E. Thierfelder, B.A. Witthuhn, A.P. McMickie, P.C. Doherty, G.C. Grosveld, J.N. Ihle, Defective lymphoid development in mice lacking Jak3, Science 270 (1995) 800;
(f) S.Y. Park, K. Saijo, T. Takahashi, M. Osawa, H. Arase, N. Hirayama, K. Miyake, H. Nakauchi, T. Shirasawa, T. Saito, Developmental defects of lymphoid cells in Jak3 kinase-deficient mice, Immunity 3 (1995) 371.

[19] a) M. Pesu, A. Laurence, N. Kishore, S.H. Zwiilich, G. Chan, J.J. O'Shea, Therapeutic targeting of Janus kinases, Immunological Reviews 223 (2008) 132;
(b) J.M. Kremer, B.J. Bloom, F.C. Breedveld, J.H. Coombs, M.P. Fletcher, D. Gruben, S. Krishnaswami, R. Burgos-Vargas, B. Wilkinson, C.A. Zerbini, S.H. Zwillich, The safety and efficacy of a JAK inhibitor in patients with cative rheumatoid arthritis: results of a double-blind, placebo-controlled phase IIa trial of three dosage levels of CP-690,550 versus placebo, Arthritis and Rheumatism 60 (2009) 1895;
(c) M.G. Boy, C. Wang, B.E. Wilkinson, V.F.-S. Chow, A.T. Clucas, J.G. Krueger, A.S. Gaweco, S.H. Zwillich, P.S. Changelian, G. Chan, Double-blind, placebo-controlled, dose-escalation study to evaluate the pharmacologic effect of CP-690,550 in patients with psoriasis, Journal of Investigative Dermatology 129 (2009) 2299.

[20] (a) C. Haan, C. Rovlering, F. Rault, M. Kapp, P. Druckes, G. Thoma, I. Behrmann, H.-G. Zerwes, Jak1 has a dominant role over JAK3 in signal transduction through γc-containing cytokine receptors, Chemistry & Biology 18 (2011) 314;
(b) G. Thoma, F. Nuninger, F. Falchetto, E. Hermes, G.A. Tavares, E. Vangrevelinghe, H.-G. Zerwes, Identification of a potent Janus kinase 3 inhibitor with high selectivity within the Janus kinase family, Journal of Medicinal Chemistry 54 (2011) 284.

[21] (a) H. Neubauer, A. Cumano, M. Muller, H. Wu, U. Huffstadt, K. Pfeffer, Jak2 deficiency defines an essential development checkpoint in definitive hematopoiesis, Cell 93 (1998) 397;
(b) E. Parganas, D. Wang, D. Stravopodis, D.J. Topharm, J.C. Marine, S. Teqlund, E.F. Vanin, S. Bodner, O.R. Colamonici, J.M. van Deursen, G. Grosveld, J.N. Ihle, Jak2 is essential for signaling through a variety of cytokine receptors, Cell 93 (1998) 385;
(c) B.A. Witthuhn, F.W. Quelle, O. Silvennoinen, T. Yi, B. Tang, O. Miura, J.N. Ihle, Jak2 associates with the erythropoietin receptor and is tyrosine phosphorylated and activated following stimulation with erythropoietin, Cell 74 (1993) 227.

[22] S.J. Sohn, K. Barrett, A. Van Abbema, C. Chang, P. Bir Kohli, H. Kanda, J. Smith, Y. Lai, A. Zhou, B. Zhang, W. Yang, K. Williams, C. Macleod, C.A. Hurley, J.J. Kulagowski, N. Lewin-Koh, H.S. Dengler, A.R. Johnson, N. Ghilardi, M. Zak, J. Liang, W.S. Blair, S. Magnuson, L.C. Wu, A restricted role for TYK2 catalytic activity in human cytokine responses, Journal of Immunology, in press.

[23] (a) M.E. Flanagan, T.A. Blumenkopf, W.H. Brissette, M.F. Brown, J.M. Casavant, C. Shang-Poa, J.L. Doty, E.A. Elliott, M.B. Fisher, M. Hines, C. Kent, E.M. Kudlacz, B.M. Littie, K.S. Magnusson, S.P. McCurdy, M.J. Munchhof, B.D. Perry, P.S. Sawyer, T.J. Strelevitz, C. Subramanyam, J. Sun, D.A. Whipple, P.S. Changelian, Discovery of CP-690,550: a potent and selective Janus kinase (JAK) inhibitor for the treatment of autoimmune diseases and organ transplant rejection, Journal of Medicinal Chemistry 53 (2010) 8468;
(b) A. Quintas-Cardama, K. Vaddi, P. Liu, T. Manshouri, J. Li, P.A. Scherle, E. Caulder, X. Wen, Y. Li, P. Waeltz, M. Rupar, T. Burn, Y. Lo, J. Kelley, M. Covington, S. Shepard, J.D. Rodgers, P. Haley, H. Kantarijian, J.S. Fridman, S. Verstovsek, Preclinical characterization of the selective Jak1/2 inhibitor INCB018424: therapeutic implications for the treatment of myeloproliferative neoplasms, Blood 115 (2010) 3109;
(c) J.E. Thompson, R.M. Cubbon, R.T. Cummings, R.F. Wicker, P.M. Cunningham, P.M. Cameron, P.T. Meinke, N. Liverton, Y. Weng, J.A. DeMartino, Photochemical preparation of a pyridone containing tetracycle: a JAK protein kinase inhibitor, Bioorganic & Medicinal Chemistry Letters 12 (2002) 1219.

[24] M. Koresawa, T. Okabe, High-throughput screening with quantitation of ATP consumption: a universal non-radioisotope, homogeneous assay for protein kinase, Assay and Drug Development Technologies 2 (2004) 153.

[25] Primary hits were defined as compounds giving > 50% inhibition at a test concentration of 5 μM in the HTS assay.

[26] (a) C. Abad-Zapatero, J.T. Metz, Ligand efficiency indices as guideposts for drug discovery, Drug Discovery Today 10 (2005) 464;
(b) A.L. Hopkins, C.R. Groom, A. Alex, Drug Discovery Today 9 (2004) 430;
(c) I.D. Kuntz, K. Chen, K.A. Sharp, P.A. Kollman, The maximal affinity of ligands, Proceedings of the National Academy of Sciences of the United States of America 96 (1999) 9997.

[27] (a) M.C. Wenlock, R.P. Austin, P. Barton, A.M. Davis, P.D. Leeson, A comparison of physiochemical property profiles of development and marketed oral drugs, Journal of Medicinal Chemistry 46 (2003) 1250;
(b) T.I. Opera, A.M. Davis, S.J. Teague, P.D. Leeson, Is there a difference between leads and drugs? A historical perspective, Journal of Chemical Information and Computer Sciences 41 (2001) 1308.

[28] *In vitro* kinase activities of purified JAK1, JAK2, and TYK2 JH1 kinase domains and the K_i values for ATP-competitive inhibition were determined as described previously: V. Tsui, P. Gibbons, M. Ultsch, K. Mortara, C. Chang, W. Blair, R. Pulk, R.M. Stanley, M. Starovasnik, D. Williams, M. Lamers, P. Leonard, S. Magnuson, J. Liang, C. Eigenbrot, A new regulatory switch in a Jak protein kinase Proteins: Structure, Function and Bioinformatics 79 (2011) 393.

[29] TYK2 biochemical selectivity is expressed as the ratio of JAK1 (Ki)/TYK2 (Ki) and JAK2 (Ki)/TYK2 (Ki). JAK3 K_i was also obtained for all analogs, but compounds were universally less potent against this isoform and so JAK3 K_i data were not included in the following SAR tables for the purpose of brevity.

[30] (a) Invitrogen, http://www.invitrogen.com/site/us/en/home.html?s_kwcid=TC|12295|invitrogen||S|e|14171840346&kw=slivgn (accessed 22.07.12).
(b) S.M. Rodems, B.D. Hamman, C. Lin, J. Zhao, S. Shah, D. Heidary, L. Makings, J.H. Stack, B.A. Pollok, Assay and Drug Development Technologies 1 (2002) 9.

[31] The steady state kinetics mechanism of inhibition for compound 1 was determined. See Supplemental data.

[32] pK_a values were calculated using the MoKa sofware(www.moldiscovery.com) and a customized pKa model. (a) F. Milletti, L. Storchi, G. Sforna, G. Cruciani, New and original pKa prediction method using grid molecular interaction fields, Journal of Chemical Information and Modeling 47 (2007) 2172;
(b) F. Milletti, L. Storchi, L. Goracci, S. Bendels, B. Wagner, M. Kansy, G. Cruciani, Extending pKa prediction accuracy: high-throughput pKa measurements to understand pKa modulation of new chemical series, European Journal of Medicinal Chemistry 45 (2010) 4270.

[33] P. Bamborough, M.J. Brown, J.A. Christopher, C. Chung, G.W. Mellor, Selectivity of kinase inhibitor fragments, Journal of Medicinal Chemistry 54 (2011) 5131. and references cited therein.

[34] The structure of TYK2 with ADP was also determined and details can be found in the Supplementary data.

[35] E.-X. Zhang, D.-X. Wang, Z.-T. Huang, M.-X. Wang, Synthesis of (NH)m(NMe) 4-m-bridged calix[4]pyridines and the effects of NH bridge on structure and properties, Journal of Organic Chemistry 74 (2009) 8595.

[36] S. Lee, M. Jorgensen, J.F. Hartwig, Palladium-catalyzed synthesis of arylamines from aryl halides and lithium bis(trimethylsilyl)amide as an ammonia equivalent, Organic Letters 3 (2001) 2729.

[37] Isopropyl amide **43** was made through Buchwald coupling of bromine **56** and 2-methyl propanamide. Details can be found in the Supplementary data.

[38] Consistent with other members of this structural class, compound **46** was not biochemically potent against JAK3 (Ki = 253 nM).

[39] Z.A. Knight, K.M. Shokat, Features of selective kinase inhibitors, Chemistry & Biology 12 (2005) 621.

[40] J.E. Chrencik, A. Patny, I.K. Leung, T.L. Emmons, T. Hall, R.A. Weinberg, J.A. Gormley, J.M. Williams, J.E. Day, J.L. Hirsch, J.R. Kiefer, J.W. Leone, H.D. Fischer, C.D. Sommers, H.-C. Huang, E.J. Jacobsen, R.E. Tenbrink, A.G. Tomasselli, T.E. Benson, Structural and thermodynamic characterization of the Tyk2 and Jak3 kinase domains in complex with CP-690550 and CMP-6, Journal of Molecular Biology 400 (2010) 413.

[41] F.H. Allen, The Cambridge structural database: a quarter of a million crystal structures and rising, Acta Crystallographica B 58 (2002) 380.

[42] (a) T. Clark, G.W. Spitznagel, R. Klose, P.V.R. Schleyer, Substituent effects on the geometries and energies of cyclopropanes and the corresponding 2-propyl derivatives, Journal of the American Chemical Society 106 (1984) 4412;
(b) R. Fuchs, J.H. Hallman, M.O. Perlman, Thermochemistry of conjugation of simple cyclopropane derivatives, Canadian Journal of Chemistry 60 (1982) 1832.

[43] (a) B. Buchmann, K. Eis, U. Bothe, A. Bonin, U. Bomer, Carbonylamino-substituierte aniline-pyromidinderivative als Tyk-inhibitoren, deren Herstellung und Verwendug als arzneimittel. DE2009001438 (2009);
(b) M.L. Boys, L.E. Burgess, R.D. Groneberg, D.M. Harvey, L. Huang, T. Kercher, C.F. Kraser, E. Laird, E. Tarlton, Q. Zhao, 5,7-Substituted-imidazo[1,2-*c*]pyrimidines as Inhibitors of JAK Kinases. WO2011130146 (2011);
(c) K. Ellard, J. Major, A. Jones, R. Lynch, N. Ramsden, Pyridine Compounds and Aza Analogs Thereof as TYK2 Inhibitors (2012). WO2012062704;
(d) T. Blench, S. Goodacre, Y. Lai, J. Liang, S. Magnuson, V.H. Tsui, K. Williams, B. Zhang, Pyrazolopyridines and Pyrazolopyridines and Their Use as Tyk2 Inhibitors (2012). WO2012066061;
(e) T. Blench, C. Ellwood, Y. Lai, J. Liang, C. MacLeod, S. Magnuson, V. Tsui, K. Williams, B. Zhang, Azabenzothiazole Compounds, Compositions and Methods of Use (2012). WO2012035039;
(f) Y. Lai, J. Liang, S. Magnuson, V.H. Tsui, B. Zhang, K.D. Robarge, Imidazopyridine Compounds, Compositions and Methods of Use (2011). WO2011113802;
(g) S.C. Goodacre, Y. Lai, J. Liang, S. Magnuson, K.D. Robarge, M.S. Stanley, V.H. Tsui, K. Williams, B. Zhang, A. Zhou, Janus Kinase Inhibitor Compounds and Methods. WO2010142752 (2010);
(h) K. Ellard, N. Ramsden, Triazolopyridines as TYK2 Inhibitors. WO2012000970 (2012).